

Inclusive Higgs boson production at the LHC in the k_T -factorization approach

N.A. Abdulov¹, A.V. Lipatov^{2,3}, M.A. Malyshev²

October 25, 2021

¹*Faculty of Physics, Lomonosov Moscow State University, 119991 Moscow, Russia*

²*Skobeltsyn Institute of Nuclear Physics, Lomonosov Moscow State University, 119991 Moscow, Russia*

³*Joint Institute for Nuclear Research, Dubna 141980, Moscow Region, Russia*

Abstract

We investigate the inclusive Higgs boson production in proton-proton collisions at the CERN LHC conditions using the k_T -factorization approach. Our analysis is based on the dominant off-shell gluon-gluon fusion subprocess (where the transverse momenta of initial gluons are taken into account) and covers $H \rightarrow \gamma\gamma$, $H \rightarrow ZZ^* \rightarrow 4l$ (where $l = e, \mu$) and $H \rightarrow W^+W^- \rightarrow e^\pm \mu^\mp \nu \bar{\nu}$ decay channels. The transverse momentum dependent (or unintegrated) gluon densities in a proton were derived from Ciafaloni-Catani-Fiorani-Marchesini equation or, alternatively, were chosen in accordance with Kimber-Martin-Ryskin prescription. We estimate the theoretical uncertainties of our calculations and compare our results with next-to-next-to-leading-order plus next-to-next-to-leading-logarithmic ones obtained using collinear QCD factorization. Our predictions agree well with the latest experimental data taken by the CMS and ATLAS Collaborations at $\sqrt{s} = 8$ and 13 TeV.

PACS number(s): 12.38.Bx, 14.80.Bn

1 Introduction

With the startup of the Large Hadron Collider (LHC), high energy physics entered a new era. A great triumph of the Standard Model (SM) is the discovery of the Higgs boson in 2012 [1,2]. The Higgs boson H was predicted more than 50 years ago as a consequence of the electroweak symmetry breaking mechanism in the SM. This mechanism introduces a single complex scalar field doublet, which gives masses to W and Z bosons and to fundamental fermions through Yukawa interaction [3–5]. The SM Higgs boson is the physical neutral scalar field which is the only remaining part of this doublet after spontaneous symmetry breaking. In extensions of SM there are additional charged and neutral scalar or pseudoscalar Higgs particles. Theoretical and experimental investigations of the Higgs boson production cross sections and its decay rates are an important test for possible deviations from the SM expectations [6–10].

Recently the CMS and ATLAS Collaborations have reported their measurements [11–16] of the inclusive Higgs boson total and differential cross sections at $\sqrt{s} = 8$ TeV in the $H \rightarrow \gamma\gamma$, $H \rightarrow ZZ^* \rightarrow 4l$ (with $l = e, \mu$) and $H \rightarrow W^+W^- \rightarrow e^\pm \mu^\mp \nu \bar{\nu}$ decay channels. Moreover, preliminary data collected at $\sqrt{s} = 13$ TeV have become available [17–20]. The measured observables, such as distributions on the transverse momentum, rapidity or scattering angle of decay particles, allow to probe fundamental properties of the Higgs boson (for example, spin and couplings to gauge bosons and fermions) and can be used to investigate the gluon dynamics in a proton since the dominant mechanism of inclusive Higgs production at the LHC is the gluon-gluon fusion¹ [6–10]. Corresponding total and differential cross sections measured at $\sqrt{s} = 8$ TeV are higher than the SM estimations, obtained at next-to-next-to-leading order (NNLO) [21–26] and matched with soft-gluon resummation carried out up to next-to-next-to-leading logarithmic accuracy (NNLL) [27,28], although no significant deviations from the perturbative Quantum Chromodynamics (pQCD) predictions² within the experimental and theoretical uncertainties are observed [11–16]. The same conclusion was made [17–20] for preliminary data taken by the CMS and ATLAS Collaborations at $\sqrt{s} = 13$ TeV. The latter were compared with the NNLOPS calculations [34,35] normalized to N³LO predictions [36–38] for gluon-gluon fusion subprocess. The NNLOPS tool provides parton-level events at NNLO accuracy and is interfaced to the PYTHIA8 event generator [39] for parton showering, hadronization and multiple parton interactions.

In the present study we give a systematic QCD analysis of the latest CMS [11–13,17,18] and ATLAS [14–16,19,20] data on the inclusive Higgs production in diphoton, four-lepton and $H \rightarrow W^+W^- \rightarrow e^\pm \mu^\mp \nu \bar{\nu}$ decay modes collected at $\sqrt{s} = 8$ and 13 TeV using the k_T -factorization approach [40,41]. The k_T -factorization approach is based on the Balitsky-Fadin-Kuraev-Lipatov (BFKL) [42] or Ciafaloni-Catani-Fiorani-Marchesini (CCFM) [43] gluon evolution equations, which resum large logarithmic terms proportional to $\ln s \sim \ln 1/x$, important at high energies (or, equivalently, at small proton longitudinal momentum fraction x carried by gluons). The CCFM equation takes into account additional terms propor-

¹The gluon-gluon fusion and weak boson fusion (namely, $qq \rightarrow qqH$ subprocess via t-channel exchange of a W or Z bosons) are also expected to be the dominant sources of semi-inclusive Higgs production at the LHC.

²The next-to-leading order perturbative electroweak corrections to the Higgs production cross section are available [29–33].

tional to $\ln 1/(1-x)$ and is almost equivalent to the BFKL equation in the limit of asymptotic energies, but also similar to the conventional Dokshitzer-Gribov-Lipatov-Altarelli-Parisi (DGLAP) [44] scenario for large x and high scale μ^2 . For inclusive Higgs production at the LHC, typical x values are $x \sim m_H/\sqrt{s} \sim 0.008 - 0.015$ (for Higgs mass $m_H \sim 125$ GeV), so that one can reach the low x domain where the BFKL-like evolution is expected to be valid. Additionally, we see certain advantages in the fact that, even with the leading-order (LO) partonic amplitudes, a large piece of higher order corrections (namely, part of NLO + NNLO + ... terms corresponding to real gluon emissions in initial state) are included by using transverse momentum dependent (TMD) gluon densities. Besides that, the latter absorb the effects of soft gluon resummation [45], that regularises the infrared divergences and makes our predictions valid even at low transverse momenta. More detailed descriptions of the k_T -factorization formalism can be found, for example, in reviews [46].

The k_T -factorization approach has been already applied to the inclusive Higgs boson production [45, 47–54]. So, the effective Lagrangian [55, 56] for the Higgs coupling to gluons (valid in the large top quark mass limit, $m_t \rightarrow \infty$) was used [45, 47, 49–54] to calculate the amplitude of dominant gluon-gluon fusion subprocess, whereas finite top mass m_t effects in the triangle quark loop were investigated [48]. The Kimber-Martin-Ryskin (KMR) [57] prescription for the TMD gluon density in a proton (where the gluon transverse momentum is generated at the last evolution step) was applied [49] and the simplified solution of the CCFM equation in the single loop approximation (where the small- x effects are neglected) was used [45]. In the framework of Monte-Carlo generator CASCADE [58] the off-shell production amplitude [50] was used with the full CCFM evolution [51]. Recently, it was demonstrated [52] that the k_T -factorization approach supplemented with the CCFM gluon dynamics is able to describe first (preliminary) data [59] on the inclusive Higgs production in the diphoton decay mode³ taken by the ATLAS Collaboration at the LHC. The effect of taking into account higher-order corrections in the k_T -factorization approach at LO was pointed out [47, 49, 52, 53]. The CMS [12] and ATLAS data [14] for Higgs boson production in the four-lepton decay mode were considered [53].

Our present consideration is based on the off-shell amplitude of the gluon-gluon fusion subprocess $g^*g^* \rightarrow H$ [47]. The latter was extended further to the subsequent diphoton [52] and four-lepton Higgs boson decays [53]. Below we will derive the expressions for off-shell $g^*g^* \rightarrow H \rightarrow W^+W^- \rightarrow e^\pm\mu^\mp\nu\bar{\nu}$ and $g^*g^* \rightarrow H \rightarrow ZZ^* \rightarrow 4l$ (where $l = e, \mu$) amplitudes (independently from [53]). Then, to calculate the Higgs boson production cross section we convolute these amplitudes with the TMD gluon densities in a proton, taken from the numerical solution of the CCFM equation [60]. As an alternative choice, we will use the TMD gluon densities evaluated in accordance with the KMR prescription [57]. Our main motivation is that the latest CMS [11, 13] and ATLAS [14, 16] data taken at $\sqrt{s} = 8$ TeV (referring to $H \rightarrow \gamma\gamma$ and $H \rightarrow W^+W^- \rightarrow e^\pm\mu^\mp\nu\bar{\nu}$ decay channels) as well as preliminary data [17–20] obtained at $\sqrt{s} = 13$ TeV have not been analysed yet in the framework of k_T -factorization. Additionally, detailed studying of the Higgs transverse momentum distributions in the different kinematical regimes of different decay channels could impose constraints on the TMD gluon density (see [47, 52, 53]).

³The preliminary ATLAS data [59] on the Higgs boson transverse momentum distribution were discussed also [54]. However, the calculations [54] are based on rather old CCFM-evolved TMD gluon density function and, in our opinion, suffer from double counting.

The outline of our paper is following. In Section 2 we recall the basic formulas of k_T -factorization approach and briefly describe the calculation steps. In Section 3 we present our numerical results and discussion. Section 4 contains our conclusions.

2 The model

Let us start from a short review of the calculation steps. We describe first the evaluation of $g^*g^* \rightarrow H \rightarrow ZZ^* \rightarrow 4l$ and $g^*g^* \rightarrow H \rightarrow W^+W^- \rightarrow e^\pm\mu^\mp\nu\bar{\nu}$ off-shell production amplitudes. The effective Lagrangian for the Higgs boson coupling to gluons in the limit of large top quark mass $m_t \rightarrow \infty$ reads [55, 56]

$$\mathcal{L}_{ggH} = \frac{\alpha_s}{12\pi} \left(G_F \sqrt{2} \right)^{1/2} G_{\mu\nu}^a G^{a\mu\nu} H, \quad (1)$$

where G_F is the Fermi coupling constant, $G_{\mu\nu}^a$ is the gluon field strength tensor and H is the Higgs scalar field. The large m_t approximation is valid to an accuracy of few percents in the mass range $m_H < 2m_t$, and, of course, is applicable at the $m_H \sim 125$ GeV [11–20]. The triangle vertex for two off-shell gluons having four-momenta k_1 and k_2 and color indices a and b thus takes the form [55, 56]:

$$T_{ggH}^{\mu\nu,ab}(k_1, k_2) = i\delta^{ab} \frac{\alpha_s}{3\pi} \left(G_F \sqrt{2} \right)^{1/2} [k_2^\mu k_1^\nu - (k_1 \cdot k_2) g^{\mu\nu}]. \quad (2)$$

Using (2) and taking into account the non-zero transverse momenta of initial gluons $k_1^2 = -\mathbf{k}_{1T}^2 \neq 0$ and $k_2^2 = -\mathbf{k}_{2T}^2 \neq 0$, one can easily obtain the off-shell production amplitudes squared for considered subprocesses. The latter can be written in a compact form:

$$|\bar{\mathcal{M}}|^2 = \frac{8}{9} \frac{\alpha_s^2}{\pi^2} G_F \sqrt{2} (4\pi\alpha)^3 m_Z^2 C_V \frac{(\hat{s} + \mathbf{p}_T^2)^2}{(\hat{s} - m_H^2)^2 + m_H^2 \Gamma_H^2} \cos^2 \phi \times \\ \times \frac{2g_{(V)L}^2 g_{(V)R}^2 (p_1 \cdot p_4)(p_2 \cdot p_3) + (g_{(V)L}^4 + g_{(V)R}^4)(p_1 \cdot p_3)(p_2 \cdot p_4)}{[(q_1^2 - m_V^2)^2 + \Gamma_V^2 m_V^2][(q_2^2 - m_V^2)^2 + \Gamma_V^2 m_V^2]}, \quad (3)$$

where we have neglected the masses of final-state leptons⁴. The symbol V denotes Z or W bosons, p_1 and p_3 are their decay leptons four-momenta, p_2 and p_4 are the antileptons four-momenta, $\hat{s} = (k_1 + k_2)^2$, the transverse momentum of the Higgs particle is $\mathbf{p}_T = \mathbf{k}_1 + \mathbf{k}_2$, Γ_H is its full decay width, ϕ is the azimuthal angle between the transverse momenta of initial gluons, q_1^2 and q_2^2 are the virtualities of the intermediate Z or W bosons, m_Z , m_W , Γ_Z and Γ_W are their masses and full decay widths, respectively. The constants C_Z and C_W are given by

$$C_Z = \frac{4}{\sin^6 2\theta_W}, \quad (4)$$

$$C_W = \frac{\cot^2 \theta_W}{64 \sin^4 2\theta_W}, \quad (5)$$

⁴We do not consider here the case of identical leptons in the final state and calculate its contribution in the same manner as for distinct leptons. This assumption is based on experimental kinematics cuts, which almost eliminate interference effects (see discussion in Section 3).

where θ_W is the Weinberg mixing angle. The left and right weak current constants read:

$$g_{(Z)L} = -\frac{1}{2} + \sin^2 \theta_W, \quad g_{(W)R} = 1, \quad (6)$$

$$g_{(Z)R} = \sin^2 \theta_W, \quad g_{(W)L} = 0. \quad (7)$$

The propagators of the intermediate Higgs and electroweak bosons are taken in the Breit-Wigner form to avoid any artificial singularities in the numerical calculations. According to the k_T -factorization prescription [40, 41], the summation over the polarizations of initial off-shell gluons is carried out with

$$\sum \epsilon^\mu \epsilon^{*\nu} = \frac{\mathbf{k}_T^\mu \mathbf{k}_T^\nu}{\mathbf{k}_T^2}. \quad (8)$$

In the limit $\mathbf{k}_T \rightarrow 0$ this expression converges to the ordinary one after averaging on the azimuthal angle. In all other respects the calculations are quite straightforward and follow the standard QCD Feynman rules. In the case of Higgs four-lepton decay $H \rightarrow ZZ^* \rightarrow 4l$, the obtained expression (3) coincides with the one [53]. The off-shell production amplitude for $g^* g^* \rightarrow H \rightarrow \gamma\gamma$ subprocess was calculated earlier [52].

To calculate the cross sections of the considered processes in the k_T -factorization approach one should convolute corresponding off-shell partonic cross sections with the TMD gluon densities in a proton. Our master formula for $H \rightarrow ZZ^* \rightarrow 4l$ and $H \rightarrow W^+ W^- \rightarrow e^\pm \mu^\mp \nu \bar{\nu}$ decay channels reads:

$$\begin{aligned} \sigma = \frac{1}{(2\pi)^8} \int \frac{\lambda^{1/2}(\hat{s}, q_1^2, q_2^2)}{512 x_1 x_2 s \hat{s} \lambda^{1/2}(\hat{s}, k_1^2, k_2^2)} f_g(x_1, \mathbf{k}_{1T}^2, \mu^2) f_g(x_2, \mathbf{k}_{2T}^2, \mu^2) |\bar{\mathcal{M}}|^2 \times \\ \times d\mathbf{k}_{1T}^2 d\mathbf{k}_{2T}^2 dy dq_1^2 dq_2^2 d\hat{s} d\Omega^* d\Omega_1^* d\Omega_2^* \frac{d\phi_1}{2\pi} \frac{d\phi_2}{2\pi}, \end{aligned} \quad (9)$$

where $f_g(x, \mathbf{k}_T^2, \mu^2)$ is the TMD gluon density, s is the total center-of-mass energy, y is the Higgs boson rapidity, Ω^* is the decay solid angle of a vector boson in the Higgs boson rest frame, Ω_1^* and Ω_2^* are the decay solid angles of produced leptons in corresponding electroweak boson rest frame, ϕ_1 and ϕ_2 are the azimuthal angles of incoming off-mass shell gluons having the fractions x_1 and x_2 of the longitudinal momenta of colliding protons, $\lambda(x, y, z)$ is the kinematical function [61]. The cross section of the inclusive Higgs production in the diphoton decay mode can be written as⁵:

$$\begin{aligned} \sigma = \frac{1}{2\pi} \int \frac{1}{16 x_1 x_2 s \lambda^{1/2}(\hat{s}, k_1^2, k_2^2)} f_g(x_1, \mathbf{k}_{1T}^2, \mu^2) f_g(x_2, \mathbf{k}_{2T}^2, \mu^2) |\bar{\mathcal{M}}|^2 \times \\ \times d\mathbf{k}_{1T}^2 d\mathbf{k}_{2T}^2 dy d\hat{s} d\Omega^* \frac{d\phi_1}{2\pi} \frac{d\phi_2}{2\pi}, \end{aligned} \quad (10)$$

where Ω^* is the decay solid angle of produced photon in the Higgs boson rest frame. This expression is more convenient for narrow Higgs resonance than the one used earlier [52].

⁵There was a missing factor 1/2 in (10) of [52], which is due to identity of the final state photons. The numerical results [52] have been corrected recently, conclusions unchanged.

Concerning the TMD gluon density functions in a proton, we have tested a few sets. First of them (JH'2013 set 2) was obtained [60] from the numerical solution of the CCFM equation. The latter seems to be the most suitable tool for our consideration because it smoothly interpolates between the small- x BFKL gluon dynamics and conventional DGLAP one, as it was mentioned above. The input parameters of starting (initial) gluon distribution were fitted to describe the high-precision DIS data on proton structure functions $F_2(x, Q^2)$ and $F_2^c(x, Q^2)$ [60]. The fit is based on TMD matrix elements and involves two-loop strong coupling constant, kinematic consistency constraint [62, 63] and non-singular terms in the CCFM gluon splitting function [64]. Below we use this TMD gluon distribution as default choice⁶. Additionally, as an alternative choice, we apply the TMD gluon density obtained from the KMR prescription [57]. The KMR approach is a formalism to construct the TMD quark and gluon densities from well-known conventional ones. The key assumption of this approach is that the k_T -dependence of the TMD parton distributions enters at the last evolution step, so that the DGLAP evolution can be used up to this step. For the input, we used Martin-Stirling-Thorn-Watt (MSTW'2008 LO) set [66].

Other essential parameters were taken as follows: the renormalization and factorization scales $\mu_R^2 = \xi^2 m_H^2$ and $\mu_F^2 = \hat{s} + \mathbf{Q}_T^2$, where \mathbf{Q}_T^2 is the transverse momentum of the incoming off-shell gluon pair⁷. To estimate the scale uncertainties of numerical calculations, we vary the unphysical parameter ξ between 1/2 and 2 about the default value $\xi = 1$. Following [67], we set electroweak bosons masses $m_Z = 91.1876$ GeV and $m_W = 80.403$ GeV, their total decay widths $\Gamma_Z = 2.4952$ GeV and $\Gamma_W = 2.085$ GeV. Additionally, we use Higgs boson mass $m_H = 126.8$ GeV, its full decay width $\Gamma_H = 4.3$ MeV, $\sin^2 \theta_W = 0.23122$ and adopt the LO formula for the strong coupling constant $\alpha_s(\mu^2)$ with $n_f = 4$ active quark flavors at $\Lambda_{\text{QCD}} = 200$ MeV, so that $\alpha_s(m_Z^2) = 0.1232$. Note that we use the running QED coupling constant $\alpha(\mu^2)$. Finally, following [49], to take into account the non-logarithmic loop corrections to the Higgs production cross section we apply the effective K -factor when using the KMR gluon density:

$$K = \exp \left[C_A \frac{\alpha_s(\mu^2)}{2\pi} \pi^2 \right], \quad (11)$$

where the color factor $C_A = 3$. A particular scale choice $\mu^2 = \mathbf{p}_T^{4/3} \hat{s}^{2/3}$ (with \mathbf{p}_T being the transverse momentum of produced Higgs boson) has been proposed [49] to eliminate sub-leading logarithmic terms. We choose this scale to evaluate the strong coupling constant in (11) only. The multidimensional integration everywhere was performed by means of a Monte Carlo technique, using the routine VEGAS [68].

3 Numerical results

Now we are in a position to present our numerical results and discussion. Let us consider first the Higgs boson production in the diphoton decay mode.

⁶At the moment, there is a large variety of proposed TMD gluon distribution functions in a proton. Most of them is collected in the TMDLIB package [65], which is a C++ library providing a framework and an interface to the different parametrizations.

⁷The special choice for μ_F scale is connected with the CCFM evolution [60].

Source	$\sigma_{\text{fid}}(\text{CMS})$ [fb]	$\sigma_{\text{fid}}(\text{ATLAS})$ [fb]
k_T -fact., JH'2013 set 2	$31.12^{+4.71}_{-0.43}$	$29.62^{+4.31}_{-0.32}$
k_T -fact., KMR	$22.47^{+11.98}_{-8.47}$	$21.38^{+11.24}_{-8.01}$
fixed-order pQCD	31^{+4}_{-3}	30.5 ± 3.3
Measurement	$32 \pm 10(\text{stat.}) \pm 3(\text{syst.})$	$43.2 \pm 9.4(\text{stat.})^{+3.2}_{-2.9}(\text{syst.}) \pm 1.2(\text{lumi.})$

Table 1: The fiducial cross sections of inclusive Higgs boson production (in the diphoton decay mode) at $\sqrt{s} = 8$ TeV. The experimental data are from CMS [11] and ATLAS [14]. The results obtained in the collinear pQCD factorization (taken from [11, 14]) are shown for comparison.

3.1 $H \rightarrow \gamma\gamma$ decay mode

All cross sections were measured in a restricted part of the phase space (fiducial phase space) defined to match the experimental acceptance in terms of the photon kinematics and topological event selection. We implemented experimental setup used by the CMS and ATLAS Collaborations in our numerical program. In the CMS analysis [11] performed at $\sqrt{s} = 8$ TeV two isolated photons originating from the Higgs boson decays are required to have pseudorapidities $|\eta^\gamma| < 2.5$. Additionally, photons with largest and next-to-largest transverse momentum p_T^γ (so-called leading and subleading photons) must satisfy the conditions of $p_T^\gamma/m^{\gamma\gamma} > 1/3$ and $p_T^\gamma/m^{\gamma\gamma} > 1/4$ respectively, where $m^{\gamma\gamma}$ is the diphoton pair mass. In the ATLAS measurement [14] performed at $\sqrt{s} = 8$ TeV both of these decay photons must have pseudorapidities $|\eta^\gamma| < 2.37$ with the leading (subleading) photon satisfying $p_T^\gamma/m^{\gamma\gamma} > 0.35$ (0.25), while invariant mass $m^{\gamma\gamma}$ is required to be $105 < m^{\gamma\gamma} < 160$ GeV. The same kinematical cuts were applied in the preliminary measurements performed by the CMS [17] and ATLAS [19] Collaborations at $\sqrt{s} = 13$ TeV with only exception that invariant mass $m^{\gamma\gamma}$ in the CMS analysis [17] should lie in the range $100 < m^{\gamma\gamma} < 180$ GeV. The diphoton pair transverse momentum $p_T^{\gamma\gamma}$, absolute value of the rapidity $|y^{\gamma\gamma}|$, photon helicity angle $\cos\theta^*$ (in the Collins-Soper frame) and difference in azimuthal angle $\Delta\phi^{\gamma\gamma}$ between the produced photons were measured [11, 14, 17, 19]. Both $p_T^{\gamma\gamma}$ and $y^{\gamma\gamma}$ probe the production mechanism and parton distribution functions in a proton, while $\cos\theta^*$ and $\Delta\phi^{\gamma\gamma}$ are related to properties (namely, spin-CP nature) of the decaying Higgs boson.

The results of our calculations are shown in Figs. 1 — 3 in comparison with the LHC data. The solid histograms were obtained with the JH'2013 set 2 gluon density by fixing both the renormalization μ_R and factorization μ_F scales at the default values, while shaded regions correspond to scale uncertainties of our predictions. Following to [60], to estimate

Source	$\sigma_{\text{fid}}(\text{CMS})$ [fb]	$\sigma_{\text{fid}}(\text{ATLAS})$ [fb]
k_T -fact., JH'2013 set 2	$69.96^{+7.11}_{-0.53}$	$68.23^{+6.69}_{-0.59}$
k_T -fact., KMR	$50.78^{+24.48}_{-17.99}$	$47.91^{+23.59}_{-17.39}$
fixed-order pQCD	75 ± 4	$62.8^{+3.4}_{-4.4}$
Measurement	$84 \pm 11(\text{stat.}) \pm 7(\text{syst.})$	$43.2 \pm 14.9(\text{stat.}) \pm 4.9(\text{syst.})$

Table 2: The fiducial cross sections of inclusive Higgs boson production (in the diphoton decay mode) at $\sqrt{s} = 13$ TeV. The preliminary experimental data are from CMS [17] and ATLAS [19]. The results obtained in the collinear pQCD factorization (taken from [17, 19]) are shown for comparison.

the latter we used the JH'2013 set 2+ and JH'2013 set 2− sets instead of default one. These two sets represent a variation of the renormalization scale used in the off-shell production amplitude. The JH'2013 set 2+ set stands for a variation of $2\mu_R$, while set JH'2013 set 2− reflects $\mu_R/2$ (see also [60] for more information). One can see that the k_T -factorization predictions reasonably agree with the LHC data within the experimental and theoretical uncertainties for all considered kinematical observables, although some tendency to slightly underestimate the ATLAS data (see Fig. 2) and CMS data at large transverse momenta $p_T^{\gamma\gamma}$ (see Fig. 1) is observed for both c.m. energies $\sqrt{s} = 8$ and 13 TeV. It could be due to the missing contributions from the weak boson fusion ($W^+W^- \rightarrow H$ and $ZZ \rightarrow H$) and/or associated HZ or HW^\pm production [54], which become important at high $p_T^{\gamma\gamma}$ and not taken into account in the present consideration. Our results for $y^{\gamma\gamma}$ and $\cos\theta^*$ distributions obtained with the JH'2013 set 2 gluon at $\sqrt{s} = 8$ TeV are consistently close to the matched NNLO + NNLL pQCD predictions obtained using the HRES routine [69] within the collinear QCD factorization (but a bit higher). Our predictions at $\sqrt{s} = 13$ TeV are similar to the NNLOPS and aMC@NLO ones⁸. It can be explained by the fact that the main part of collinear QCD higher-order corrections (namely, NLO + NNLO + N³LO + ... contributions which correspond to the $\log 1/x$ enhanced terms in perturbative series) are effectively taken into account as a part of the CCFM gluon evolution⁹. A similar observation was done earlier [47, 49, 52] and confirmed recently [53]. The calculations based on the alternative KMR gluon density also tend to underestimate the ATLAS data at small $p_T^{\gamma\gamma}$, although they describe well the CMS data and ATLAS data at high transverse momenta. Moreover, we find that these predictions (mainly for distributions in $y^{\gamma\gamma}$ or $\cos\theta^*$) are generally similar to the lower uncertainty bounds of matched NNLO + NNLL (and NNLOPS or aMC@NLO)

⁸We take these predictions from the CMS [11, 14] and ATLAS [17, 19] papers.

⁹The conventional high-order QCD corrections are known to be large, of about 80 – 100% [6–9].

pQCD calculations. This can be explained from the fact that the KMR procedure absorbs only single gluon emission at the last step of evolution (or, in other words, initial state gluon emission closest to the produced Higgs boson), that corresponds to taking into account of $\ln 1/x$ enhanced NLO contributions only. One can see that the shapes of $y^{\gamma\gamma}$ or $\cos\theta^*$ distributions calculated using the CCFM-evolved and KMR gluon densities practically coincide and therefore the difference between the JH'2013 set 2 and KMR predictions for these observables can illustrate the role of conventional high-order contributions above the NLO level. Here we demonstrate again the main advantage of the k_T -factorization approach, which gives us the possibility to estimate the size of higher-order corrections and reproduce in a straightforward manner the main features of cumbersome fixed-order pQCD calculations. In contrast, one can see that the shapes of $p_T^{\gamma\gamma}$ distributions predicted by the JH'2013 set 2 and KMR gluon densities are very different from each other. Of course, it is not surprising since the Higgs boson transverse momentum is strongly related to the initial gluon transverse momenta [45, 47–53]. The importance of this observable to distinguish between the different non-collinear evolution scenarios was pointed out [47, 52, 53]. Moreover, the difference in azimuthal angle $\Delta\phi^{\gamma\gamma}$ is also very sensitive to the initial gluon transverse momenta (see Fig. 1). Such sensitivity is well-known and was demonstrated earlier for number of processes (see, for example, [46] and references therein). Thus, we confirm the previous conclusions [47, 52, 53] that these observables can impose constraints on the TMD gluon densities of the proton.

The estimated Higgs boson fiducial cross sections at $\sqrt{s} = 8$ and 13 TeV are listed in Tables 1 and 2 in comparison with the available data and conventional high-order pQCD calculations performed using the HRES [69], NNLOPS [34, 35] and aMC@NLO [70] tools. One can see that the k_T -factorization predictions are close to corresponding fixed-order collinear pQCD results and agree well with the LHC data within the theoretical and experimental uncertainties. The scale dependence of the k_T -factorization predictions (especially obtained with the KMR gluon density) is significant and exceeds the uncertainties of conventional fixed-order pQCD calculations (which are about of 10 – 11%)¹⁰. However, it could be easily understood because only the tree-level LO hard scattering amplitudes are involved. Moreover, it was argued [58] that amending the leading-logarithmic evolution with different kinematical constraints should lead to reasonable QCD predictions, although still formally only in leading logarithmic accuracy (see also [46]).

3.2 $H \rightarrow ZZ^* \rightarrow 4l$ and $H \rightarrow W^+W^- \rightarrow e^\pm\mu^\mp\nu\bar{\nu}$ decay channels

Now we turn to the $H \rightarrow ZZ^* \rightarrow 4l$ and $H \rightarrow W^+W^- \rightarrow e^\pm\mu^\mp\nu\bar{\nu}$ decay channels. The data for the first of them come from the CMS [12] and ATLAS Collaborations [15]. In the ATLAS analysis [15] done at $\sqrt{s} = 8$ TeV only events with a four-lepton invariant mass $118 < m_{4l} < 129$ GeV are kept and each lepton (electron or muon) must satisfy transverse momentum cut $p_T > 6$ GeV and be in the pseudorapidity range $|\eta| < 2.47$. The highest- p_T lepton in the quadruplet must have $p_T > 20$ GeV and the second (third) lepton in p_T order must satisfy $p_T > 15(10)$ GeV. These leptons are required to be separated from each other by $\Delta R = \sqrt{(\Delta\eta)^2 + (\Delta\phi)^2} > 0.1(0.2)$ when having the same (different) lepton flavors. The invariant mass m_{12} of the lepton pair closest to the Z boson mass (leading pair) is

¹⁰Note that scale uncertainties of the CCFM-based predictions are comparable with the ones of higher-order collinear pQCD calculations.

required to be $50 < m_{12} < 106$ GeV. The subleading pair is chosen as the remaining lepton pair with invariant mass m_{34} closest to the Z boson mass and satisfying the requirement $12 < m_{34} < 115$ GeV. The CMS measurement [12] performed at the same energy $\sqrt{s} = 8$ TeV requires at least four leptons in the event with at least one lepton having $p_T > 20$ GeV, another lepton having $p_T > 10$ GeV and the remaining ones having $p_T > 7$ and 5 GeV respectively. All leptons must have the pseudorapidity $|\eta| < 2.4$, the leading pair invariant mass m_{12} must be $40 < m_{12} < 120$ GeV and subleading one should be $12 < m_{34} < 120$ GeV. Finally, the four-lepton invariant mass m_{4l} must satisfy $105 < m_{4l} < 140$ GeV cut. Such cuts allow one to identify the decay leptons as originating from different Z bosons (real and virtual) and the interference effects in case of the production of identical leptons thus can be neglected¹¹. Similar to the diphoton decay, the measurements are performed in several observables related to the Higgs boson production and decay, namely the Higgs transverse momentum p_T^H and rapidity $|y^H|$, invariant mass of the subleading lepton pair m_{34} and cosine of the leading lepton pair decay angle $|\cos \theta^*|$ in the four-lepton rest frame with respect to the beam axis. While the distributions in the p_T^H and $|y^H|$ observables are sensitive to the production mechanism and gluon densities in a proton, the distributions in the decay variables m_{34} and $|\cos \theta^*|$ are sensitive to the Lagrangian structure of Higgs interaction (spin/CP quantum numbers and higher-dimensional operators). In the ATLAS analysis [16] performed at $\sqrt{s} = 8$ TeV for the $H \rightarrow W^+W^- \rightarrow e^\pm \mu^\mp \nu \bar{\nu}$ decay channel, events are selected from those with exactly one electron and one muon with opposite charge, a dilepton invariant mass $10 < m_{ll} < 55$ GeV, azimuthal angle difference $\Delta\phi^{ll} < 1.8$ and missing transverse momentum (which is produced by the two neutrinos from the W boson decays) $p_T^{\text{miss}} > 20$ GeV. The leading lepton is required to have $p_T > 22$ GeV, the other one is required to have $p_T > 15$ GeV and both of them should be in the range $|\eta| < 2.47$. The CMS analysis [13] requires $p_T > 20(10)$ GeV for the leading (subleading) leptons with $|\eta| < 2.5$, lepton pair invariant mass $m_{ll} > 12$ GeV, their transverse momentum $p_T^{ll} > 30$ GeV and invariant mass of the leptonic system in the transverse plane $m_T^{ll\nu\nu} > 50$ GeV. The differential cross sections were measured as functions of Higgs boson transverse momentum p_T^H and absolute value of the dilepton rapidity $|y^{ll}|$. The latter is highly correlated to the Higgs boson rapidity y^H which can not be reconstructed experimentally in the $H \rightarrow W^+W^- \rightarrow e^\pm \mu^\mp \nu \bar{\nu}$ final state. Of course, all the experimental cuts listed above are taken into account in the numerical evaluations. The preliminary data reported by the CMS [18] and ATLAS [20] Collaborations at $\sqrt{s} = 13$ TeV were obtained using similar analysis strategy.

The results of our calculations are shown in Figs. 4 — 8 in comparison with the data. The estimated total cross sections are listed in Tables 3 — 5. Similar to $H \rightarrow \gamma\gamma$ decay, the k_T -factorization predictions for $H \rightarrow ZZ^* \rightarrow 4l$ and $H \rightarrow W^+W^- \rightarrow e^\pm \mu^\mp \nu \bar{\nu}$ decay modes agree well with the LHC data taken at $\sqrt{s} = 8$ TeV for all considered kinematical observables within the theoretical and experimental uncertainties. The best description of the data is achieved with the CCFM-evolved JH'2013 set 2 gluon density. Moreover, the overall agreement between these predictions and the preliminary ATLAS data [20] taken at $\sqrt{s} = 13$ TeV looks to be even a bit better than the one given by the NNLO pQCD calculations (see Fig. 8), that could be essentially due to the small- x region probed. The KMR approach results in lower cross sections compared to the JH'2013 set 2 calculations since

¹¹Incorrect identification is possible but happens only approximately in 5% of events [15].

Source	$\sigma_{\text{fid}}(\text{CMS})$ [fb]	$\sigma_{\text{fid}}(\text{ATLAS})$ [fb]
k_T -fact., JH'2013 set 2	$1.61^{+0.22}_{-0.01}$	$1.58^{+0.23}_{-0.01}$
k_T -fact., KMR	$1.22^{+0.59}_{-0.42}$	$1.20^{+0.58}_{-0.43}$
fixed-order pQCD	$1.15^{+0.12}_{-0.13}$	1.30 ± 0.13
Measurement	$1.11^{+0.41}_{-0.35}(\text{stat.})^{+0.14}_{-0.10}(\text{syst.})^{+0.08}_{-0.02}(\text{mod.})$	$2.11^{+0.53}_{-0.47}(\text{stat.}) \pm 0.08(\text{syst.})$

Table 3: The fiducial cross sections of inclusive Higgs production (in the $H \rightarrow ZZ^* \rightarrow 4l$ decay channel) at $\sqrt{s} = 8$ TeV. The experimental data are from CMS [12] and ATLAS [15]. The results obtained in the collinear pQCD factorization (taken from [12, 15]) are shown for comparison.

Source	$\sigma_{\text{fid}}(\text{CMS})$ [fb]	$\sigma_{\text{fid}}(\text{ATLAS})$ [fb]
k_T -fact., JH'2013 set 2	$54.47^{+8.20}_{-0.46}$	$34.02^{+5.58}_{-0.38}$
k_T -fact., KMR	$40.80^{+21.33}_{-15.06}$	$27.38^{+13.07}_{-9.39}$
fixed-order pQCD	48 ± 8	25.1 ± 2.6
Measurement	$39 \pm 8(\text{stat.}) \pm 9(\text{syst.})$	$36.0 \pm 7.2(\text{stat.}) \pm 6.4(\text{syst.}) \pm 1.0(\text{lumi.})$

Table 4: The fiducial cross sections of inclusive Higgs production (in the $H \rightarrow W^+W^- \rightarrow e^\pm \mu^\mp \nu \bar{\nu}$ decay channel) at $\sqrt{s} = 8$ TeV. The experimental data are from CMS [13] and ATLAS [16]. The results obtained in the collinear pQCD factorization (taken from [13, 16]) are shown for comparison.

Source	$\sigma_{\text{fid}}(\text{CMS})$ [fb]	$\sigma_{\text{fid}}(\text{ATLAS})$ [fb]
k_T -fact., JH'2013 set 2	$3.61^{+0.33}_{-0.01}$	$3.84^{+0.38}_{-0.02}$
k_T -fact., KMR	$2.71^{+1.17}_{-0.90}$	$2.83^{+1.28}_{-0.96}$
fixed-order pQCD	2.76 ± 0.14	2.91 ± 0.13
Measurement	$2.92^{+0.48}_{-0.44}(\text{stat.})^{+0.28}_{-0.24}(\text{syst.})$	$3.62^{+0.53}_{-0.50}(\text{stat.})^{+0.25}_{-0.20}(\text{syst.})$

Table 5: The fiducial cross sections of inclusive Higgs production (in the $H \rightarrow ZZ^* \rightarrow 4l$ decay channel) at $\sqrt{s} = 13$ TeV. The preliminary experimental data are from CMS [18] and ATLAS [20]. The results obtained in the collinear pQCD factorization (taken from [18, 20]) are shown for comparison.

only single gluon emission in the initial state is taken into account here. Good agreement is also observed in the normalized differential cross sections $1/\sigma d\sigma/dp_T^H$ and $1/\sigma d\sigma/d|y^\ell|$ (see Fig. 7). Studying of the normalized differential cross sections leads to a more stringent comparison between data and theory due to reduced experimental (mainly systematic) uncertainties. As it was expected, the distributions on the Higgs boson transverse momentum are highly sensitive to the TMD gluon densities applied in the numerical calculations and therefore can be used to discriminate between the latter. In contrast, the predicted shapes of rapidity and $\cos\theta^*$ distributions are almost insensitive to the TMD gluon density in a proton. The KMR predictions for these distributions are rather similar to the lower uncertainty bounds of the NNLOPS calculations, whereas the JH'2013 set 2 ones slightly overshoot them. This fact demonstrates again the role of $\ln 1/x$ -enhanced NNLO + N³LO + ... terms taken into account in the CCFM gluon evolution.

Finally, we would like to note that a similar study (but using the $H \rightarrow ZZ^* \rightarrow 4l$ decay channel only) was done very recently [53]. Unlike our choice, older version of CCFM-evolved gluon density in a proton (namely, set A0) [72] was applied in these calculations. We reproduce the results [53] when using the A0 gluon.

4 Conclusions

We investigated the inclusive Higgs boson production in pp collisions at the LHC using the $H \rightarrow \gamma\gamma$, $H \rightarrow ZZ^* \rightarrow 4l$ and $H \rightarrow W^+W^- \rightarrow e^\pm\mu^\mp\nu\bar{\nu}$ decay channels in the framework of the k_T -factorization approach. Our consideration was based on the dominant off-shell gluon-gluon fusion subprocess where the transverse momenta of initial gluons are taken into account. The essential part of our analysis was using of the TMD gluon density derived

from the CCFM evolution equation. The latter seems to be the most suitable tool for our consideration because it smoothly interpolates between the small- x BFKL gluon dynamics and conventional DGLAP one, which is valid at large Bjorken x . Using the CCFM-evolved gluon density, we have achieved reasonably good description of the latest data taken by the CMS and ATLAS Collaborations at $\sqrt{s} = 8$ TeV and recent preliminary data taken at $\sqrt{s} = 13$ TeV. The theoretical uncertainties of our calculations were estimated and comparison with the high-order pQCD predictions (up to NNLO + NNLL level) obtained within the collinear factorization was done. We have illustrated the effect of taking into account $\ln 1/x$ -enhanced higher-order terms in our calculations and demonstrated the strong sensitivity of predicted Higgs transverse momentum distributions to the TMD gluon densities used. Such observables could impose constraints on the latter.

5 Acknowledgements

We would like to thank S.P. Baranov, H. Jung, V. Rawoot and R. Islam for their very useful discussions and important remarks. This research was supported in part by RFBR grant 16-32-00176-mol-a and grant of the President of Russian Federation NS-7989.2016.2. We are grateful to DESY Directorate for the support in the framework of Moscow — DESY project on Monte-Carlo implementation for HERA — LHC. M.A.M. was also supported by a grant of the foundation for the advancement of theoretical physics "Basis" 17-14-455-1.

References

- [1] CMS Collaboration, Phys. Lett. B **716**, 30 (2012).
- [2] ATLAS Collaboration, Phys. Lett. B **716**, 1 (2012).
- [3] P.W. Higgs, Phys. Rev. Lett. **13**, 508 (1964);
F. Englert, R. Brout, Phys. Rev. Lett. **13**, 321 (1964);
G.S. Gunalnik, C.R. Hagen, T.W.B. Kibble, Phys. Rev. Lett. **13**, 585 (1964).
- [4] S.L. Glashow, Nucl. Phys. **22**, 579 (1961).
- [5] S. Weinberg, Phys. Rev. Lett. **19**, 1264 (1967).
- [6] LHC Higgs Cross Section Working Group, arXiv:1101.0593 [hep-ph].
- [7] LHC Higgs Cross Section Working Group, arXiv:1201.3084 [hep-ph].
- [8] LHC Higgs Cross Section Working Group, arXiv:1307.1347 [hep-ph].
- [9] LHC Higgs Cross Section Working Group, arXiv:1610.07922 [hep-ph].
- [10] P. Cipriano, S. Dooling, A. Grebenyuk, P. Gunnellini, F. Hautmann, H. Jung, P. Katsas, arXiv:1308.1655 [hep-ph].
- [11] CMS Collaboration, Eur. Phys. J. C **76**, 13 (2016).

- [12] CMS Collaboration, JHEP **04**, 005 (2016).
- [13] CMS Collaboration, JHEP **03**, 032 (2017).
- [14] ATLAS Collaboration, JHEP **09**, 112 (2014).
- [15] ATLAS Collaboration, Phys. Lett. B **738**, 234 (2014).
- [16] ATLAS Collaboration, JHEP **08**, 104 (2016).
- [17] CMS Collaboration, CMS note CMS-PAS-HIG-17-015.
- [18] CMS Collaboration, CMS note CMS-PAS-HIG-16-041.
- [19] ATLAS Collaboration, ATLAS note ATLAS-CONF-2016-067.
- [20] ATLAS Collaboration, arXiv:1708.02810 [hep-ex]; ATLAS note ATLAS-CONF-2017-032.
- [21] M. Spira, A. Djouadi, D. Graudenz, P. Zerwas, Nucl. Phys. B **453**, 17 (1995).
- [22] A. Djouadi, M. Spira, P.M. Zerwas, Phys. Lett. B **264**, 440 (1991).
- [23] S. Dawson, Nucl. Phys. B **359**, 283 (1991).
- [24] R.V. Harlander, W.B. Kilgore, Phys. Rev. Lett. **88**, 201801 (2002).
- [25] C. Anastasiou, K. Melnikov, Nucl. Phys. B **646**, 220 (2002).
- [26] V. Ravindran, J. Smith, W.L. van Neerven, Nucl. Phys. B **665**, 325 (2003).
- [27] S. Catani, D. de Florian, M. Grazzini, P. Nason, JHEP **0307**, 028 (2003).
- [28] D. de Florian, G. Ferrera, M. Grazzini, D. Tommasini, JHEP **1111**, 064 (2011).
- [29] U. Aglietti, R. Bonciani, G. Degrossi, A. Vicini, Phys. Lett. B **595**, 432 (2004).
- [30] S. Actis, G. Passarino, C. Sturm, S. Uccirati, Phys. Lett. B **670**, 12 (2008).
- [31] D. de Florian, M. Grazzini, Phys. Lett. B **718**, 117 (2012).
- [32] C. Anastasiou, S. Buehler, F. Herzog, A. Lazopoulos, JHEP **1204**, 004 (2012).
- [33] J. Baglio, A. Djouadi, JHEP **1103**, 055 (2011).
- [34] K. Hamilton, P. Nason, E. Re, G. Zanderighi, JHEP **1310**, 222 (2013).
- [35] K. Hamilton, P. Nason, G. Zanderighi, JHEP **1505**, 140 (2015).
- [36] C. Anastasiou, C. Duhr, F. Dulat, F. Herzog, B. Mistlberger, Phys. Rev. Lett. **114**, 212001 (2015).

- [37] C. Anastasiou, C. Duhr, F. Dulat, E. Furlan, T. Gehrmann, F. Herzog, A. Lazopoulos, B. Mistlberger, JHEP **05**, 058 (2016).
- [38] C. Anastasiou, R. Boughezal, F. Petriello, JHEP **04**, 003 (2009).
- [39] T. Sjöstrand, S. Ask, J.R. Christiansen, R. Corke, N. Desai, P. Ilten, S. Mrenna, S. Prestel, C.O. Rasmussen, P.Z. Skands, Comput. Phys. Commun. **191**, 159 (2015).
- [40] L.V. Gribov, E.M. Levin, M.G. Ryskin, Phys. Rep. **100**, 1 (1983);
E.M. Levin, M.G. Ryskin, Yu.M. Shabelsky, A.G. Shuvaev, Sov. J. Nucl. Phys. **53**, 657 (1991).
- [41] S. Catani, M. Ciafaloni, F. Hautmann, Nucl. Phys. B **366**, 135 (1991);
J.C. Collins, R.K. Ellis, Nucl. Phys. B **360**, 3 (1991).
- [42] E.A. Kuraev, L.N. Lipatov, V.S. Fadin, Sov. Phys. JETP **44**, 443 (1976);
E.A. Kuraev, L.N. Lipatov, V.S. Fadin, Sov. Phys. JETP **45**, 199 (1977);
I.I. Balitsky, L.N. Lipatov, Sov. J. Nucl. Phys. **28**, 822 (1978).
- [43] M. Ciafaloni, Nucl. Phys. B **296**, 49 (1988);
S. Catani, F. Fiorani, G. Marchesini, Phys. Lett. B **234**, 339 (1990);
S. Catani, F. Fiorani, G. Marchesini, Nucl. Phys. B **336**, 18 (1990);
G. Marchesini, Nucl. Phys. B **445**, 49 (1995).
- [44] V.N. Gribov and L.N. Lipatov, Sov. J. Nucl. Phys. **15**, 438 (1972);
L.N. Lipatov, Sov. J. Nucl. Phys. **20**, 94 (1975);
G. Altarelli, G. Parisi, Nucl. Phys. B **126**, 298 (1977);
Yu.L. Dokshitzer, Sov. Phys. JETP **46**, 641 (1977).
- [45] A. Gawron, J. Kwiecinski, Phys. Rev. D **70**, 014003 (2004).
- [46] B. Andersson *et al.* (Small- x Collaboration), Eur. Phys. J. C **25**, 77 (2002);
J. Andersen *et al.* (Small- x Collaboration), Eur. Phys. J. C **35**, 67 (2004);
J. Andersen *et al.* (Small- x Collaboration), Eur. Phys. J. C **48**, 53 (2006).
- [47] A.V. Lipatov, N.P. Zotov, Eur. Phys. J. C **44**, 559 (2005).
- [48] R.S. Pasechnik, O.V. Teryaev, A. Szczurek, Eur. Phys. J. C **47**, 429 (2006).
- [49] G. Watt, A.D. Martin, M.G. Ryskin, Phys. Rev. D **70**, 014012 (2004).
- [50] F. Hautmann, Phys. Lett. B **535**, 159 (2002).
- [51] H. Jung, Mod. Phys. Lett. A **19**, 1 (2004).
- [52] A.V. Lipatov, M.A. Malyshev, N.P. Zotov, Phys. Lett. B **735**, 79 (2014);
A.V. Lipatov, M.A. Malyshev, N.P. Zotov, in Proceedings of the 22th International Workshop on High Energy Physics and Quantum Field Theory (QFTHEP'2015), Samara, Russia (2015).

- [53] R. Islam, M. Kumar, V.S. Rawoot, arXiv:1706.01402 [hep-ph].
- [54] A. Szczurek, M. Luszczak, R. Maciula, Phys. Rev. D **90**, 094023 (2014).
- [55] J.R. Ellis, M.K. Gaillard, D.V. Nanopoulos, Nucl. Phys. B **106**, 292 (1976).
- [56] M.A. Shifman, A.I. Vainshtein, M.B. Voloshin, V.I. Zakharov, Sov. J. Nucl. Phys. **30**, 711 (1979).
- [57] M.A. Kimber, A.D. Martin, M.G. Ryskin, Phys. Rev. D **63**, 114027 (2001);
G. Watt, A.D. Martin, M.G. Ryskin, Eur. Phys. J. C **31**, 73 (2003).
- [58] H. Jung, S.P. Baranov, M. Deak, A. Grebenyuk, F. Hautmann, M. Hentschinski,
A. Knutsson, M. Kraemer, K. Kutak, A.V. Lipatov, N.P. Zotov, Eur. Phys. J. C **70**,
1237 (2010).
- [59] ATLAS Collaboration, ATLAS note ATLAS-CONF-2013-072.
- [60] F. Hautmann, H. Jung, Nucl. Phys. B **883**, 1 (2014).
- [61] E. Bycling, K. Kajantie, Particle Kinematics, John Wiley and Sons (1973).
- [62] J. Kwiecinski, A.D. Martin, P. Sutton, Z. Phys. C **71**, 585 (1996).
- [63] B. Andersson, G. Gustafson, J. Samuelsson, Nucl. Phys. B **467**, 443 (1996).
- [64] M. Hansson, H. Jung, arXiv:hep-ph/0309009.
- [65] <http://tmd.hepforge.org>
- [66] A.D. Martin, W.J. Stirling, R.S. Thorne, G. Watt, Eur. Phys. J. C **63**, 189 (2009).
- [67] PDG Collaboration, Chin. Phys. C **38**, 090001 (2014).
- [68] G.P. Lepage, J. Comput. Phys. **27**, 192 (1978).
- [69] M. Grazzini, H. Sargsyan, JHEP **09**, 129 (2013).
- [70] J. Alwall, R. Frederix, S. Frixione, V. Hirschi, F. Maltoni, O. Mattelaer, H.-S. Shao,
T. Stelzer, P. Torrielli, M. Zaro, JHEP **07**, 079 (2014).
- [71] K. Hamilton, P. Nason, G. Zanderighi, JHEP **10**, 155 (2012).
- [72] H. Jung, arXiv:hep-ph/0411287.

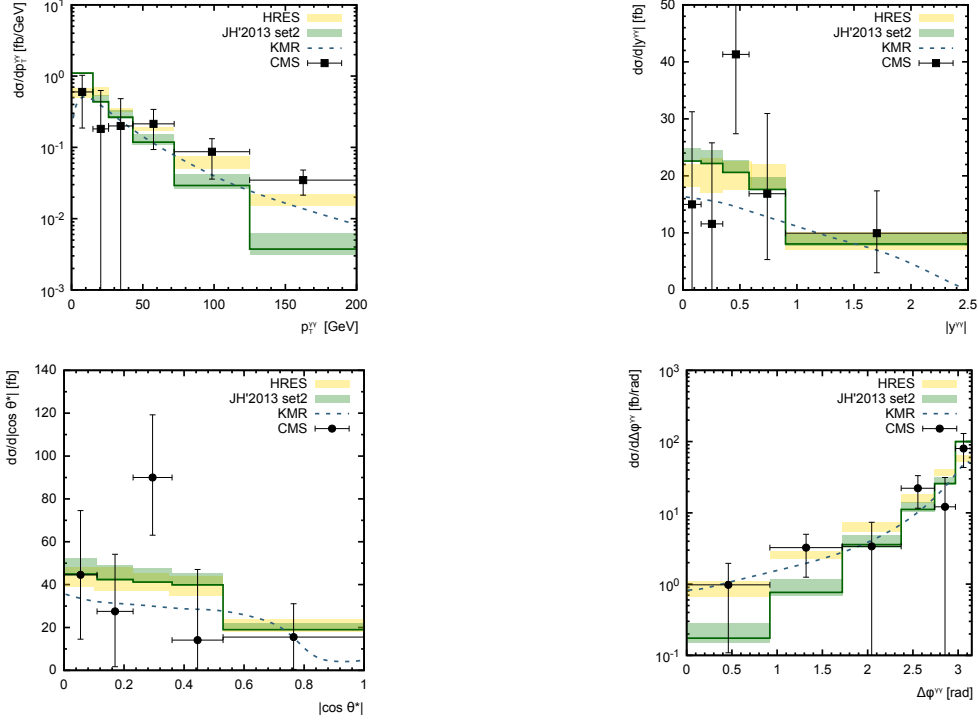


Figure 1: The differential cross sections of inclusive Higgs boson production (in the diphoton decay mode) at $\sqrt{s} = 8$ TeV as functions of diphoton pair transverse momentum $p_T^{\gamma\gamma}$, rapidity $|y^{\gamma\gamma}|$, azimuthal angle difference $\Delta\phi^{\gamma\gamma}$ and photon helicity angle $\cos\theta^*$ (in the Collins-Soper frame). The solid histograms represent the k_T -factorization predictions obtained with the JH'2013 set 2 gluon density at the default hard scales. The shaded bands (green) represent the scale uncertainties of these calculations, as it is described in the text. The dashed curves correspond to the calculations with the KMR gluon density. The NNLO + NNLL pQCD predictions obtained using the HRES routine [69] (taken from [11]) are presented as a hatched (blue) band. The experimental data are from CMS [11].

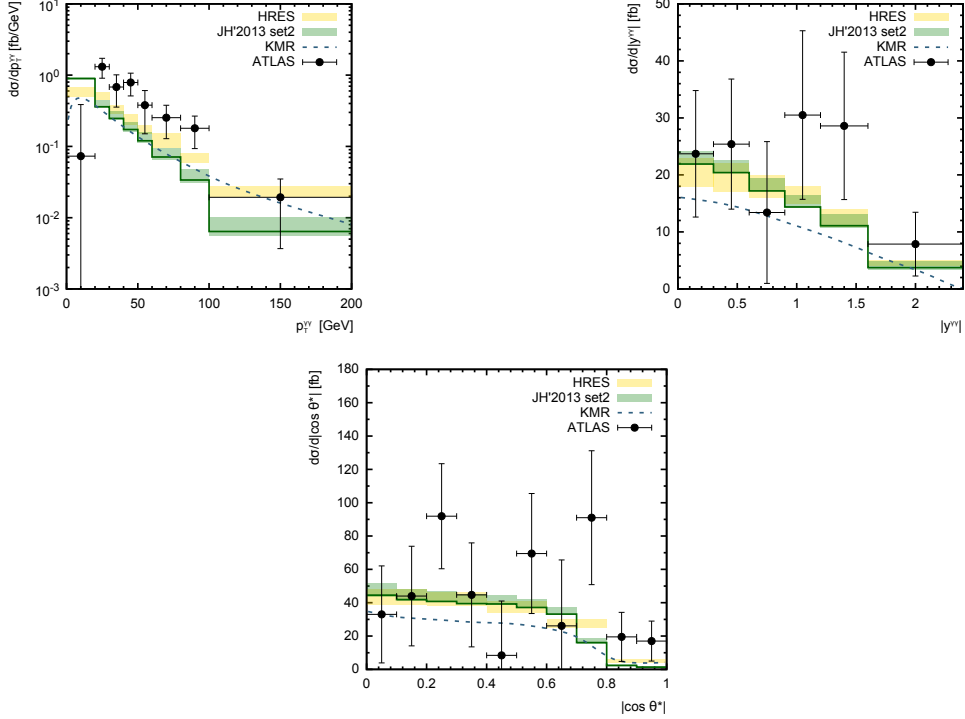


Figure 2: The differential cross sections of inclusive Higgs boson production (in the diphoton decay mode) at $\sqrt{s} = 8$ TeV as functions of diphoton pair transverse momentum $p_T^{\gamma\gamma}$, rapidity $|y^{\gamma\gamma}|$ and photon helicity angle $\cos \theta^*$ in the Collins-Soper frame. Notation of histograms and curves is the same as in Fig. 1. The experimental data are from ATLAS [14]. The HRES [69] predictions are taken from [14].

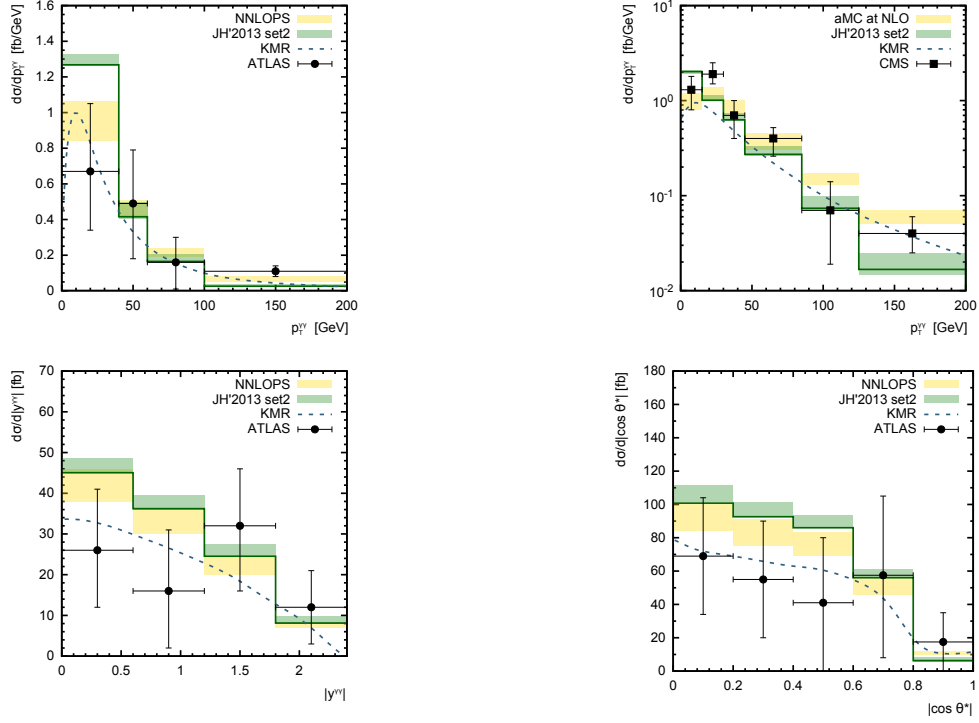


Figure 3: The differential cross sections of inclusive Higgs boson production (in the diphoton decay mode) at $\sqrt{s} = 13$ TeV as functions of diphoton pair transverse momentum $p_T^{\gamma\gamma}$, rapidity $|y^{\gamma\gamma}|$ and photon helicity angle $\cos \theta^*$ in the Collins-Soper frame. Notation of histograms and curves is the same as in Fig. 1. The preliminary experimental data are from CMS [17] and ATLAS [19]. The NNLOPS [34,35] and aMC@NLO [70] predictions are taken from [17,19].

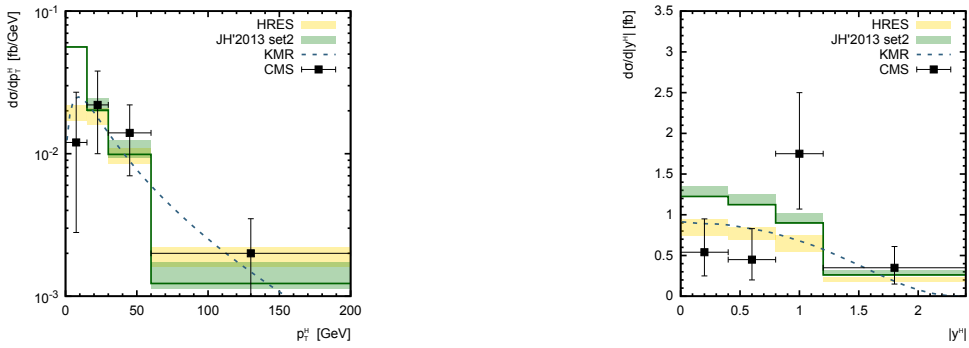


Figure 4: The differential cross sections of inclusive Higgs boson production (in the $H \rightarrow ZZ^* \rightarrow 4l$ decay mode) at $\sqrt{s} = 8$ TeV as functions of Higgs transverse momentum and rapidity. Notation of histograms and curves is the same as in Fig. 1. The experimental data are from CMS [12]. The HRES [69] predictions are taken from [12].

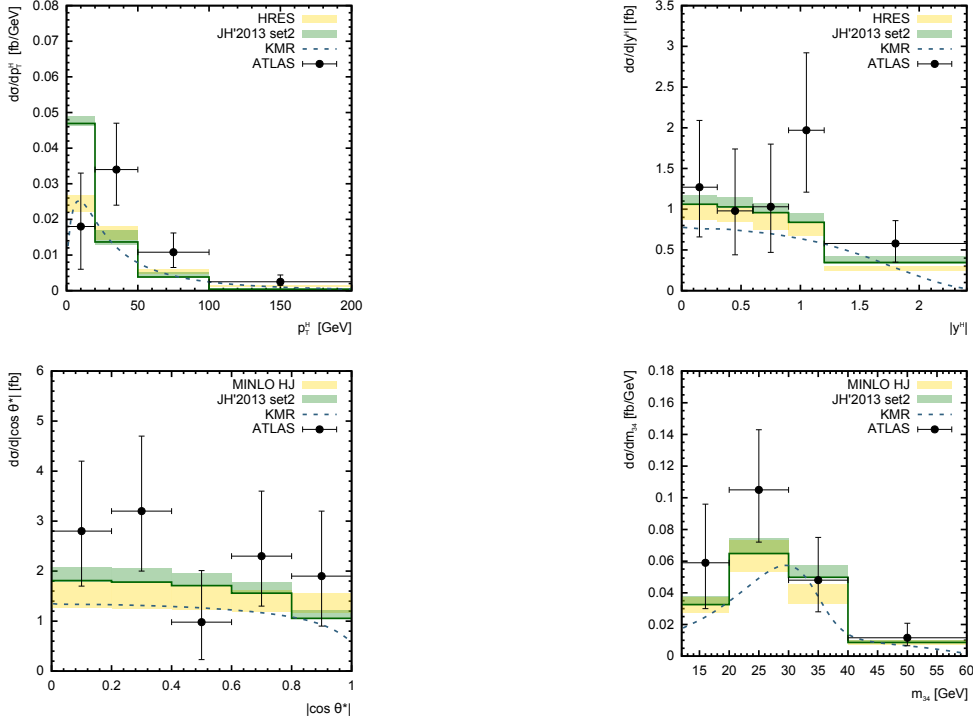


Figure 5: The differential cross sections of inclusive Higgs boson production (in the $H \rightarrow ZZ^* \rightarrow 4l$ decay mode) at $\sqrt{s} = 8$ TeV as functions of Higgs transverse momentum p_T^H , rapidity $|y^H|$, leading lepton pair decay angle $\cos \theta^*$ (in the Collins-Soper frame) and invariant mass m_{34} of subleading lepton pair. Notation of histograms and curves is the same as in Fig. 1. The experimental data are from ATLAS [15]. The HRES [69] and MINLO HJ [71] predictions are taken from [15].

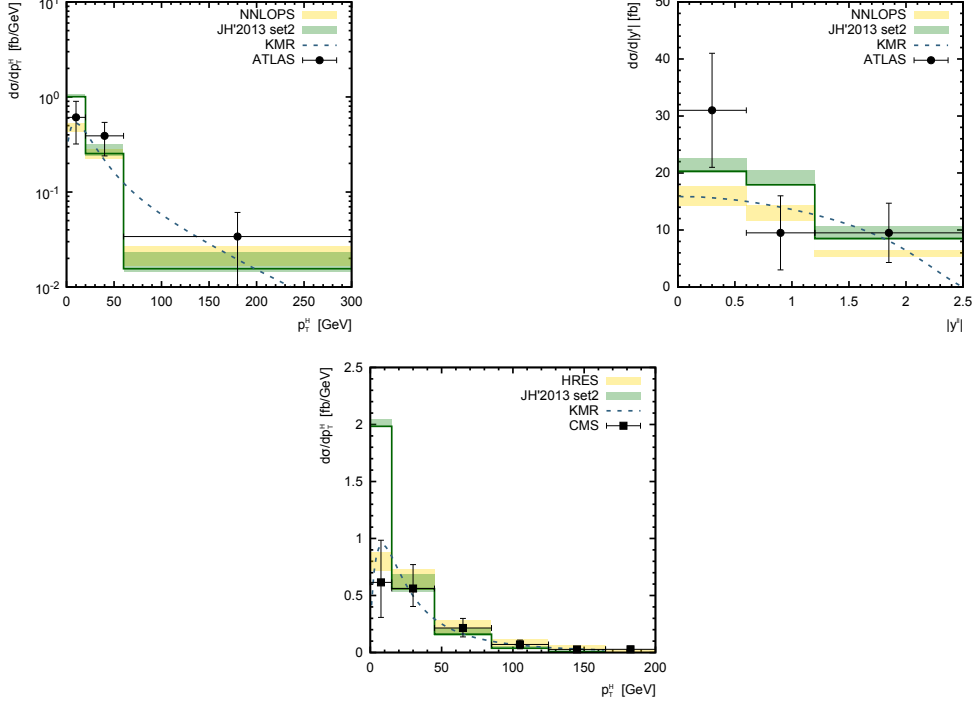


Figure 6: The differential cross sections of inclusive Higgs production (in the $H \rightarrow W^+W^- \rightarrow e^\pm\mu^\mp\nu\bar{\nu}$ decay mode) at $\sqrt{s} = 8$ TeV as functions of Higgs transverse momentum and lepton pair rapidity. Notation of histograms and curves is the same as in Fig. 1. The experimental data are from CMS [13] and ATLAS [16]. The HRES [69] and NNLOPS [34, 35] predictions are taken from [13, 16].

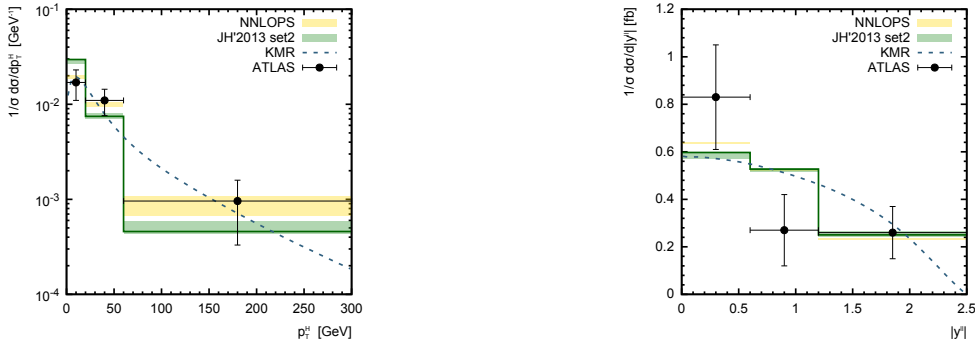


Figure 7: The normalized differential cross sections of inclusive Higgs production (in the $H \rightarrow W^+W^- \rightarrow e^\pm\mu^\mp\nu\bar{\nu}$ decay mode) at $\sqrt{s} = 8$ TeV as functions of Higgs transverse momentum and lepton pair rapidity. Notation of histograms and curves is the same as in Fig. 1. The experimental data are from ATLAS [16]. The NNLOPS [34, 35] predictions are taken from [16].

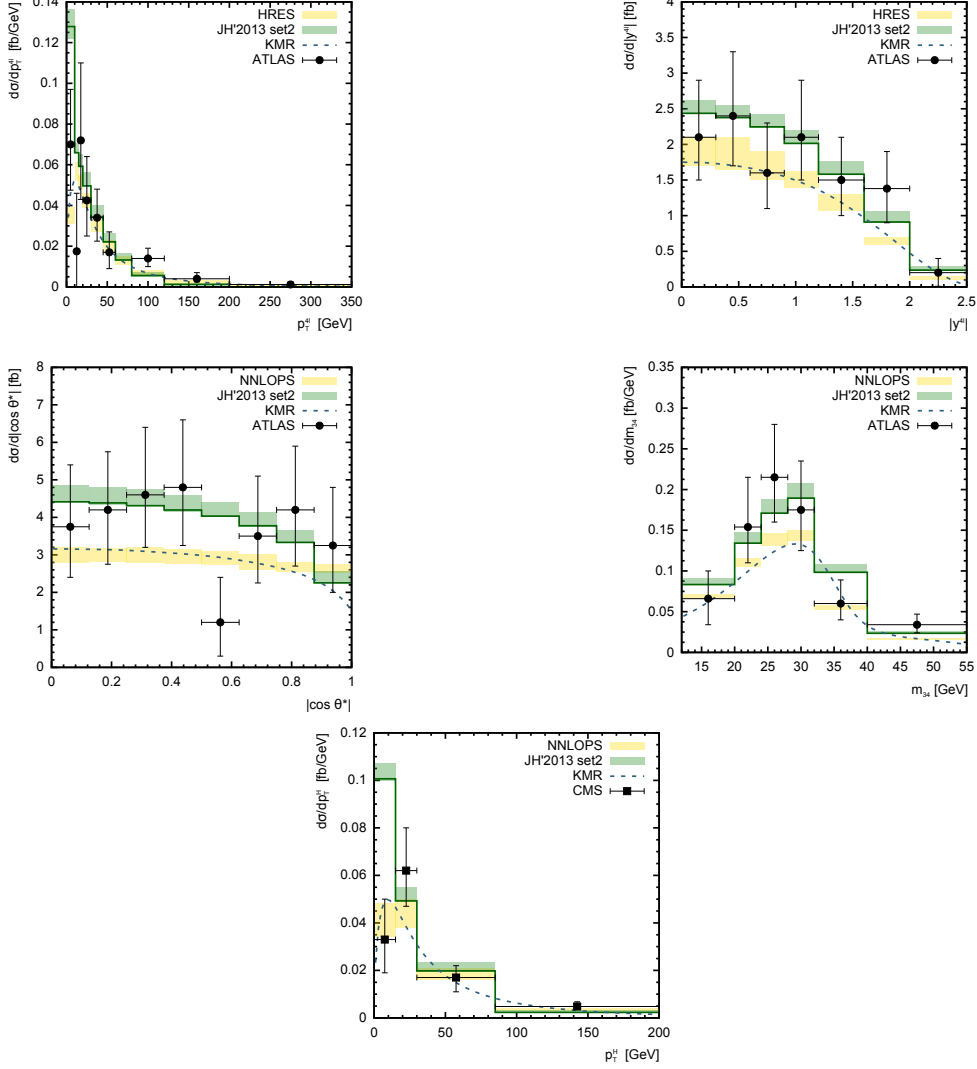


Figure 8: The differential cross sections of inclusive Higgs production (in the $H \rightarrow ZZ^* \rightarrow 4l$ decay mode) at $\sqrt{s} = 13$ TeV as functions of Higgs boson transverse momentum p_T^H , rapidity $|y^H|$, leading lepton pair decay angle $\cos \theta^*$ (in the Collins-Soper frame) and invariant mass m_{34} of the subleading lepton pair. Notation of histograms and curves is the same as in Fig. 1. The preliminary experimental data are from CMS [18] and ATLAS [20]. The HRES [69] and NNLOPS [34, 35] predictions are taken from [18, 20].